SUPPLEMENTARY INFORMATION

Antimicrobial α-defensins as Multi-target Inhibitors Against Amyloid Formation and Microbial Infection

Yanxian Zhang[1ζ], Yonglan Liu[1ζ], Yijing Tang[1], Dong Zhang[1], Huacheng He[2], Jiang Wu[3], and Jie Zheng[1*]

[1]Department of Chemical, Biomolecular, and Corrosion Engineering
The University of Akron, Ohio, USA

[2]College of Chemistry and Materials Engineering
Wenzhou University, Zhejiang, China

[3]School of Pharmaceutical Sciences
Wenzhou Medical University, Zhejiang, China

[ζ] The authors contribute equally to this work.

[*] Corresponding author: zhengj@uakron.edu

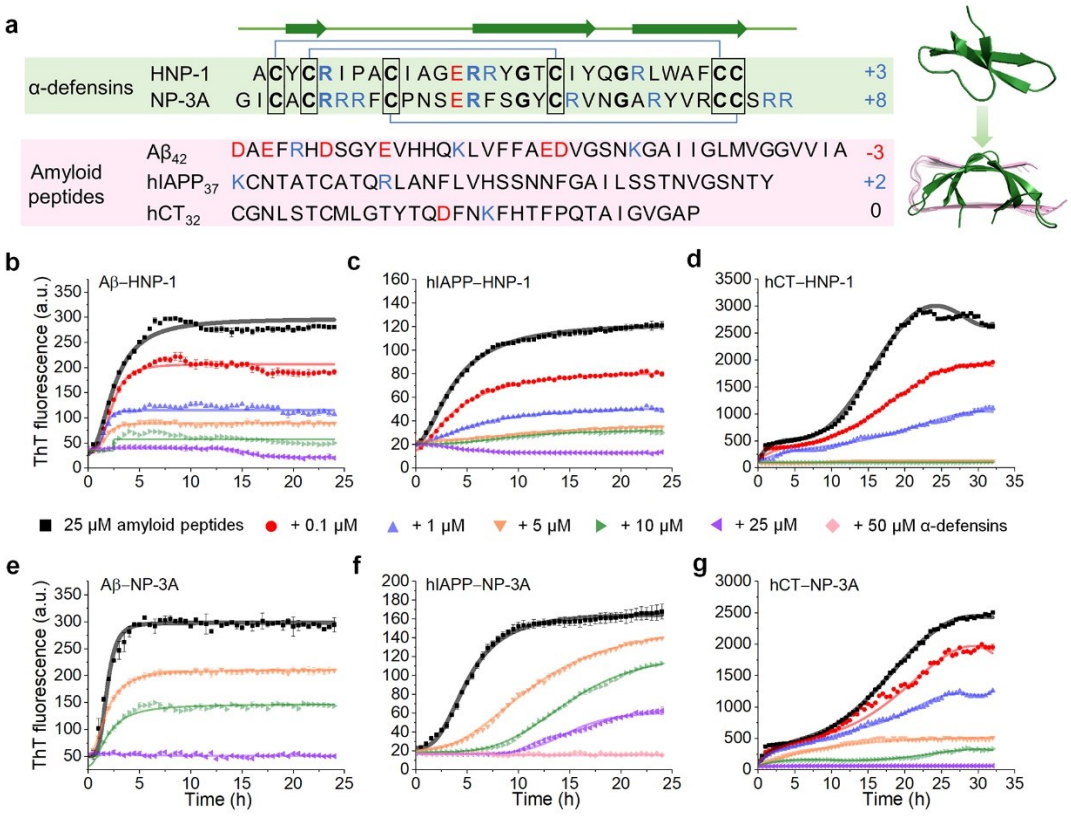

Figure S1. β-structure rich α-defensins inhibit the aggregation of amyloid peptides. a Sequences of α-defensin HNP-1 and NP-3A, and amyloid peptides A□, hIAPP, and hCT. (red: negative charged residues. blue: positive charged residues. bold: identical residues.) Kinetic aggregation profiles of **b, e** 25 μM Aβ, **c, f** 25 μM hIAPP, **d, g** 25 μM hCT in the absence (black) or presence of (b-d) HNP-1 and (e-g) NP-3A at different concentrations, followed by ThT fluorescence assay. All data represent mean ± standard error of triplicate measurements.

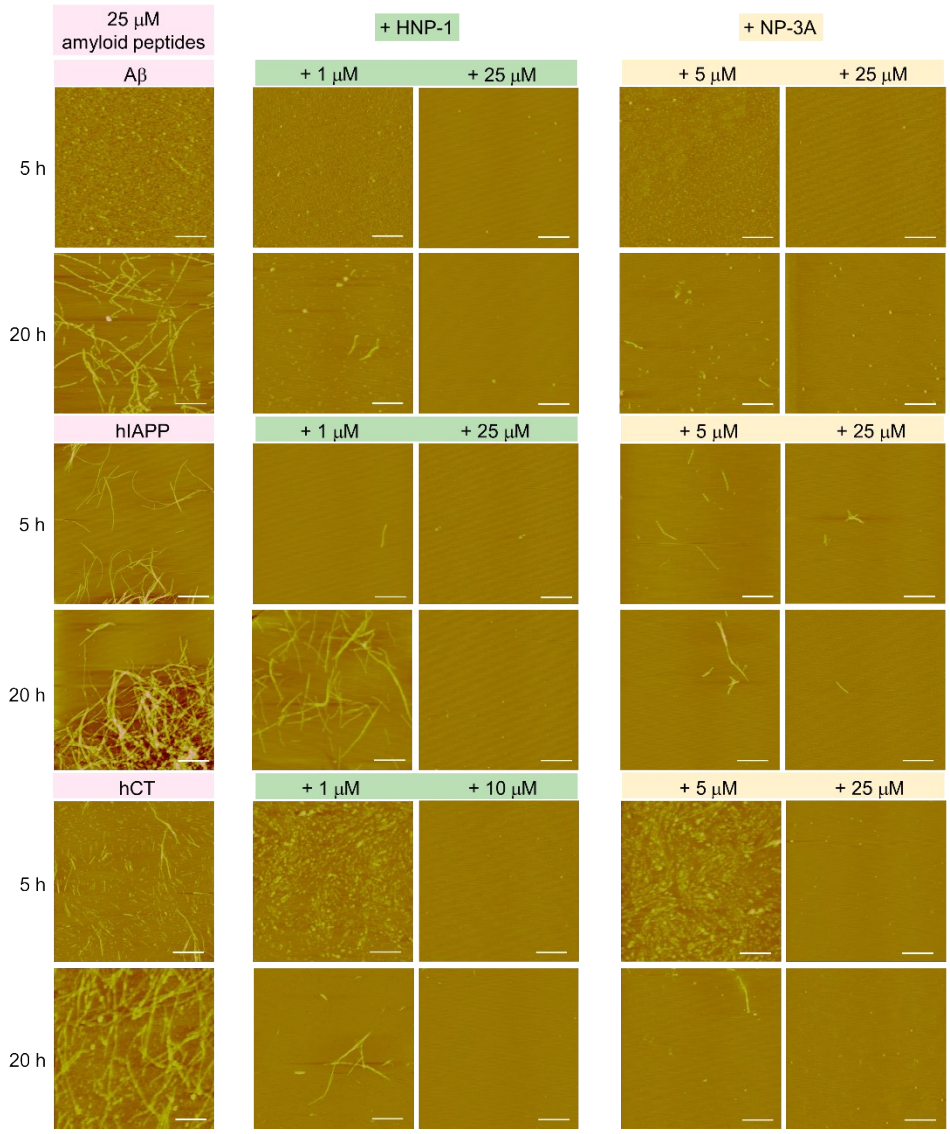

Figure S2. α-defensins suppress the formation of amyloid aggregates. AFM characterization of the morphological changes of 25 μM amyloid Aβ, hIAPP and hCT, in the absence (left column) and presence of α-defensin HNP-1 (middle column) and NP-3A (right column) at different concentrations after 5 h and 20 h incubation. Scale bars=1 μm.

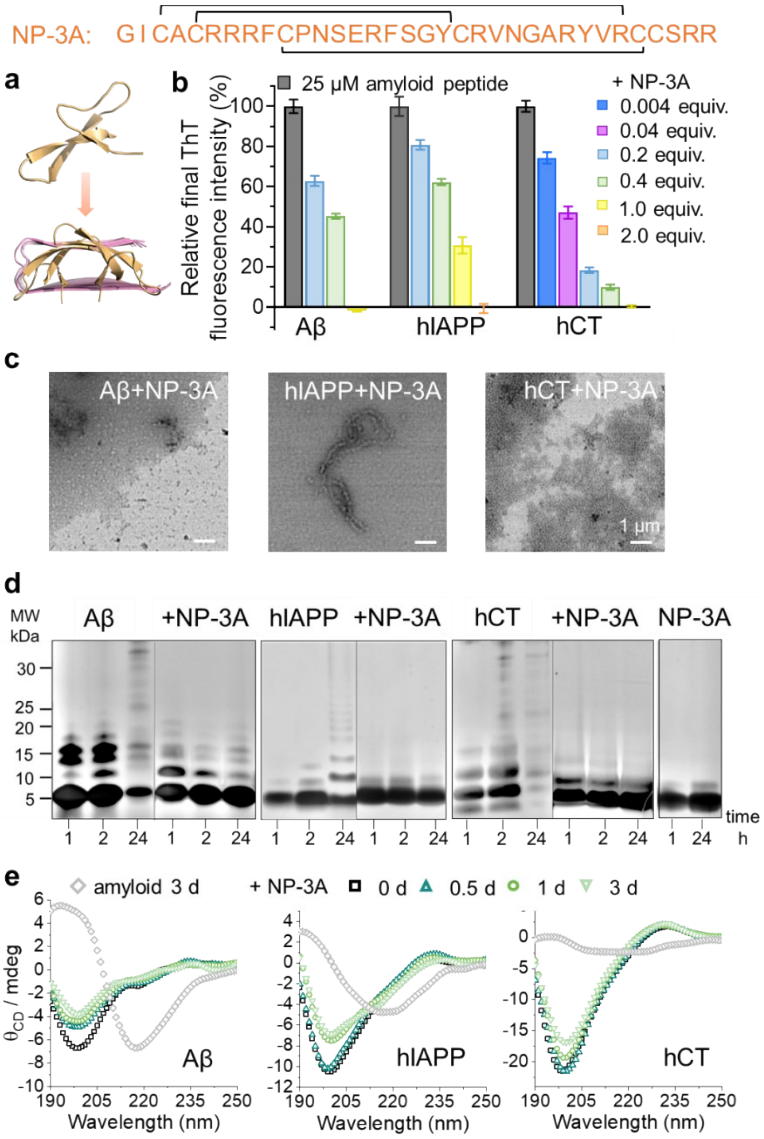

Figure S3. NP-3A exhibits a general inhibition property against the fibrillization of different amyloid peptides. **a** Sequence and structure of α-defensin NP-3A with β-rich structure. **b** Dose-dependent inhibition effect of NP-3A on Aβ, hIAPP, and hCT aggregation followed by ThT fluorescence assays. Inhibition efficiency of NP-3A is determined by the relative final fluorescence intensity (%) as normalized by that of pure amyloid aggregation. Equivalent value of NP-3A is defined by the molar ratio of NP-3A:amyloid peptide. Error bar represents the standard deviation (s.d.) of triplicate measurements. **c** TEM image of 25 μM Aβ, hIAPP, and hCT in the presence of an equimolar concentration of NP-3A. Samples were prepared after 3 days incubation in physiological environment (pH 7.4, 37 °C). Scale bars=200 nm. **d** SDS-PAGE characterization of 25 μM Aβ, hIAPP, and hCT homo-/hetero-assemblies in the absence or presence of 25 μM NP-3A. **e** Circular dichroism (CD) spectra of 25 μM Aβ, hIAPP, hCT in the absence (gray diamond, control) or in the presence of NP-3A at 0- , 0.5-, 1- and 3-days incubation. NP-3A was added to Aβ or hCT solution at 25 μM, but to hIAPP solution at 50 μM.

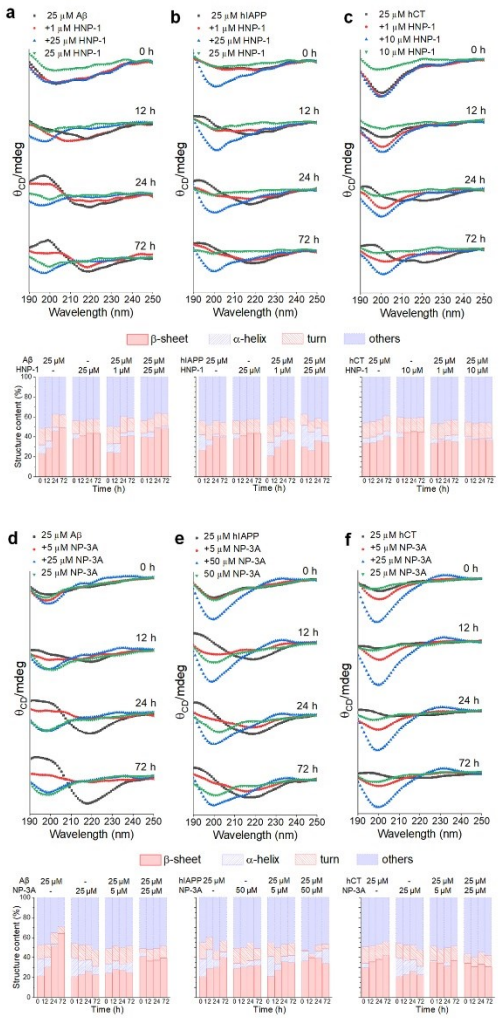

Figure S4. α-defensins inhibit the conformational change of amyloid peptides. CD spectra and the corresponding secondary structure contents calculated for **a,d** 25 μM Aβ, **b,e** 25 μM hIAPP, **c,f** 25 μM hCT in the absence (black square, control) or presence of (a-c) HNP-1 and (d-f) NP-3A at 0-, 0.5-, 1- and 3-days incubation.

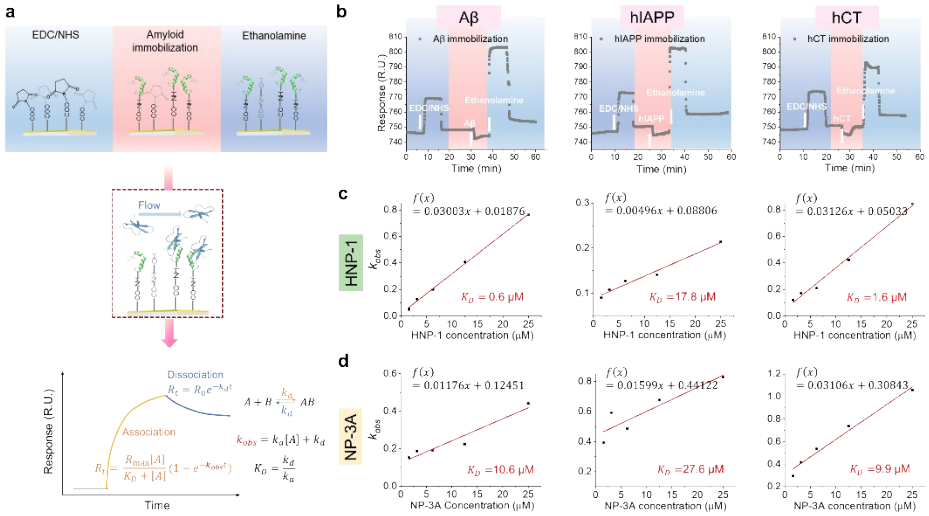

Figure S5. Binding affinity between α-defensins and amyloid peptides determined by SPR analysis. a Schematic illustration of the immobilization of amyloid peptides onto SPR chip via EDC/NHS coupling method, and the characteristic association-dissociation sensorgram phases to determine observable binding constant (k_{obs}), association constant (k_a), dissociation constant (k_d), and binding constant (K_D= k_d/k_a) based on 1:1 Langmuir model. **b** SPR sensorgrams of the immobilization of Aβ, hIAPP and hCT amyloid peptides on SPR chips. Binding constant (K_D) of α-defensins **c** HNP-1 and **d** NP-3A to amyloid peptides calculated from SPR sensorgrams (Fig. 2a and Fig. S6a) by fitting observable binding constant k_{obs} to α-defensins concentrations.

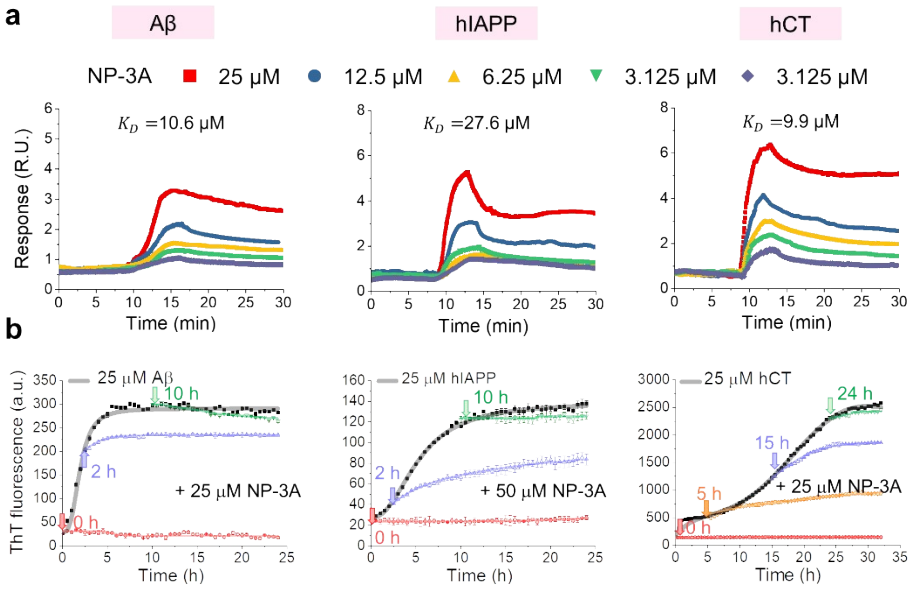

Figure S6. NP-3A binds to amyloid aggregates and inhibits further aggregation. a SPR sensorgrams of the concentration-dependent binding of NP-3A to Aβ-, hIAPP-, and hCT-coated surface. Binding affinity between NP-3A and amyloid peptides is determined by binding constant (K_D) as calculated based on 1:1 Langmuir model (Fig. S5). **b** Inhibition effect of NP-3A on Aβ, hIAPP, and hCT seeds formed at different time-points followed by ThT fluorescence assay. NP-3A was added to amyloid solution at different aggregation phases as indicated by arrows.

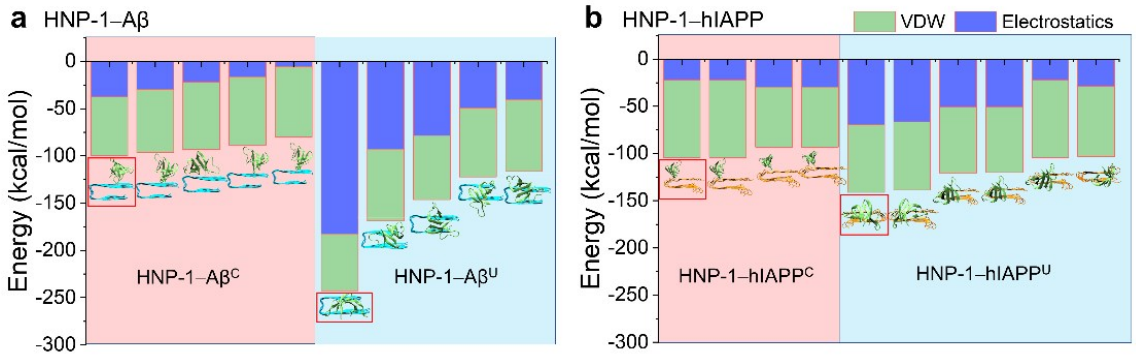

Figure S7. Determination of binding modes of α-defensins to amyloid peptides. Nonbonded interaction energies and the decomposed components of electrostatic and VDW potentials between HNP-1 and **a** Aβ or **b** hIAPP for different binding modes of HNP-1–Aβ (HNP-1–$A\beta^{C}$ and HNP-1–$A\beta^{U}$) or HNP-1–hIAPP (HNP-1–$hIAPP^{C}$ and HNP-1–$hIAPP^{U}$). We applied the two docking programs of Patchdock and Firedock to (i) search the top favorable binding complexes of antimicrobial and amyloid peptides, (ii) then we classified them into the two binding patterns, i.e., binding to beta-sheet region and binding to U-turn region, and (iii) next we used the docking structures as initial configurations to run MD simulations for examining their binding stability.

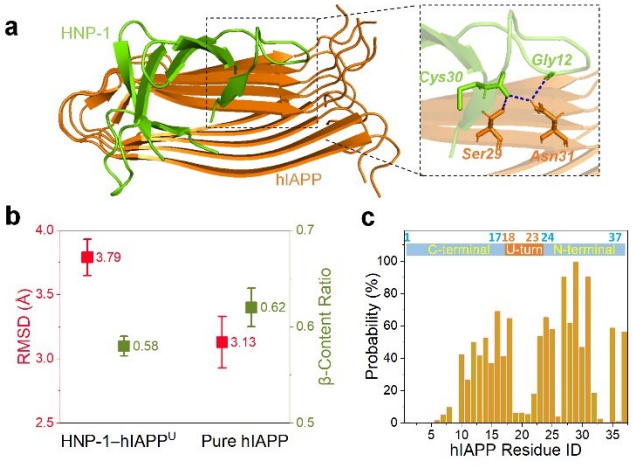

Figure S8. Binding of HNP-1 to U-turn regions of hIAPP prevents the elongation and disturbs amyloid aggregates of hIAPP. a Final snapshot of binding of HNP-1 to U-turn region of hIAPP and close-up hydrogen bond between HNP-1 and hIAPP at HNP-1–hIAPP interface for HNP-1–hIAPP^{U} model. **b** Comparison of RMSD (red) and β-content ratio (green) of hIAPP in HNP-1–hIAPP^{U} and pure hIAPP models. **c** Binding probability (%) of hIAPP residues to HNP-1 for HNP-1–hIAPP^{U} model.

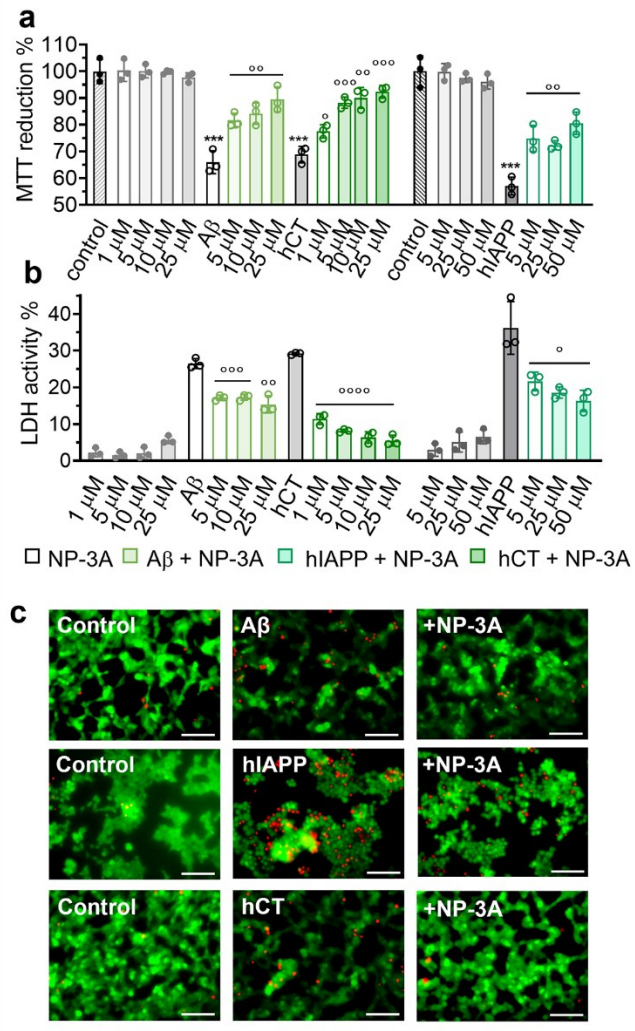

Figure S9. NP-3A rescue mammalian cells from amyloid-induced cell toxicity. Dose-dependent protection effect of NP-3A against amyloid Aβ-, hCT-, and hIAPP-induced **a** cellular toxicity as revealed by MTT assay, and **b** cell membrane disruption as revealed by LDH assay. Cells were incubated with amyloid peptides (25 μM) for 24 h in the absence or presence of 1-50 μM NP-3A. Untreated cells were set as control (100% MTT reduction and 0% LDH activity), cells after lysis were set for 100% LDH activity, and cells only incubated with NP-3A (grey bars) were also analyzed for comparison. All data represent mean ± s.d. of three independent experiments. Statistical analysis (n = 3) was conducted for cells treated with NP-3A or amyloid peptides alone relative to control (°, $p < 0.05$; °°, $p < 0.01$; °°°, $p < 0.001$), and cells treated with both NP-3A and amyloid peptides relative to cells treated with amyloid peptides alone (∗, $p < 0.05$; ∗∗, $p < 0.01$; ∗∗∗, $p < 0.001$). **c** Representative fluorescence microscopy images of cells treated for 3 h with freshly prepared amyloid peptides (25 μM) in the absence or presence of 5 μM NP-3A. Untreated cells were set as control. Red and green fluorescence indicate the dead and live cells, respectively. Scale bars=100 μm.

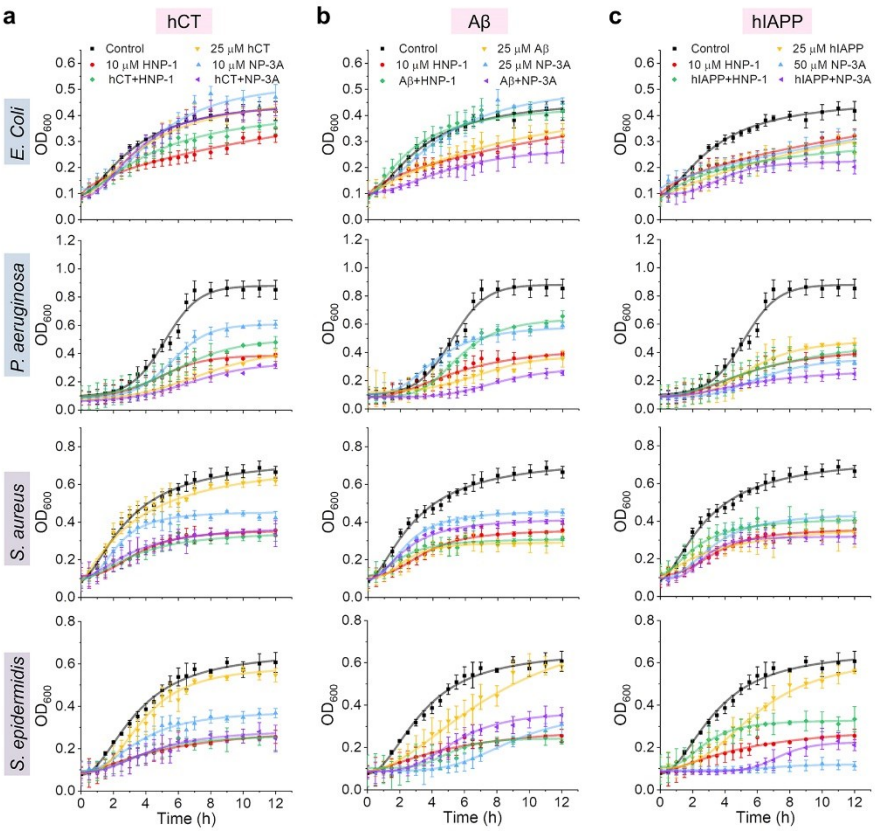

Figure S10. Antimicrobial activity of α-defensins, amyloid peptides, and cross-species of α-defensins–amyloid peptides against Gram-negative and Gram-positive bacteria. Growth profiles of representative Gram-negative bacteria *E. coli* and *P. aeruginosa*, Gram-positive bacteria *S. aureus* and S. *epidermidis* cultured in the absence and presence of **a** 10 μM HNP-1, 10 μM NP-3A, 25 μM hCT, **b** 10 μM HNP-1, 25 μM NP-3A, 25 μM Aβ, and **c** 10 μM HNP-1, 50 μM NP-3A, 25 μM hIAPP, as well as corresponding α-defensins–amyloid peptides.

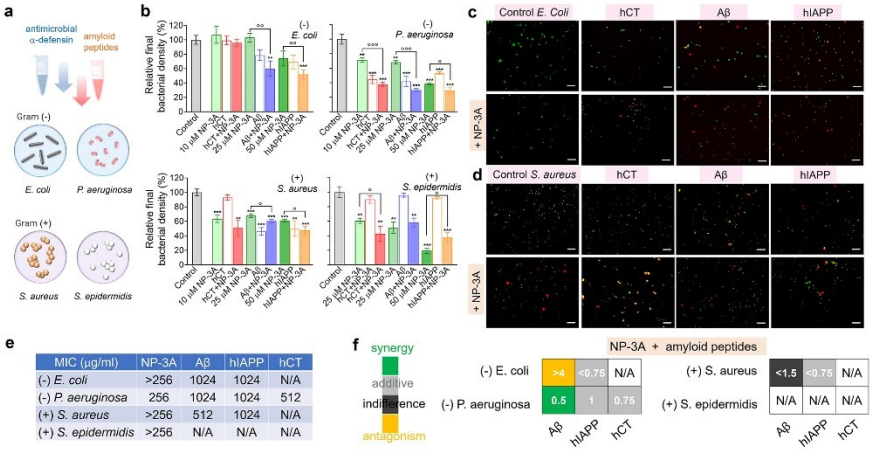

MIC (μg/ml)	NP-3A	Aβ	hIAPP	hCT
(-) *E. coli*	>256	1024	1024	N/A
(-) *P. aeruginosa*	256	1024	1024	512
(+) *S. aureus*	>256	512	1024	N/A
(+) *S. epidermidis*	>256	N/A	N/A	N/A

Figure S11. Cross-species of NP-3A–amyloid peptides retain a broad-spectrum antimicrobial activity against both Gram-negative and Gram-positive bacteria. a Cross-cooperative antimicrobial activity was assessed by exposing both Gram-negative (*E. coli*, *P. aeruginosa*) and Gram-positive bacteria (*S. aureus*, *S. epidermidis*) to mixtures of α-defensins and amyloid peptides for 12 h. **b** Antimicrobial activity of NP-3A (10-50 μM), amyloid peptides (25 μM), and cross-species of NP-3A–amyloid peptides against Gram-negative *E. Coli* and *P. aeruginosa*, Gram-positive *S. aureus* and S. epidermidis quantified by final bacterial density. Bacterial density is determined by OD_{600} and relative final bacterial density (%) treated with peptides is calculated in comparison with untreated control (100%). Statistical analysis (n = 3) was conducted relative to control (*, $p < 0.05$; **, $p < 0.01$; ***, $p < 0.001$) and bacteria treated with NP-3A (°, $p < 0.05$; °°, $p < 0.01$). Representative fluorescence microscopy images of the **c** Gram-negative *E. coli* bacteria and **d** Gram-positive *S. aureus* bacteria treated with or without peptides (25 μM amyloid peptides, 50 μM NP-3A) for 1 h. Green and red fluorescence indicate the live and dead bacteria, respectively. Scale bars=20 μm. **e** Minimal inhibitory concentration (MIC) of NP-3A and amyloid peptides against bacteria. **f** Fractional inhibitory concentration (FIC) index of the combination of NP-3A and amyloid peptides as calculated from checkerboard assay in Figure S12. Synergy (FIC≤0.5), additive (0.5<FIC<1), indifferent (1<FIC≤4), antagonism (FIC>4).

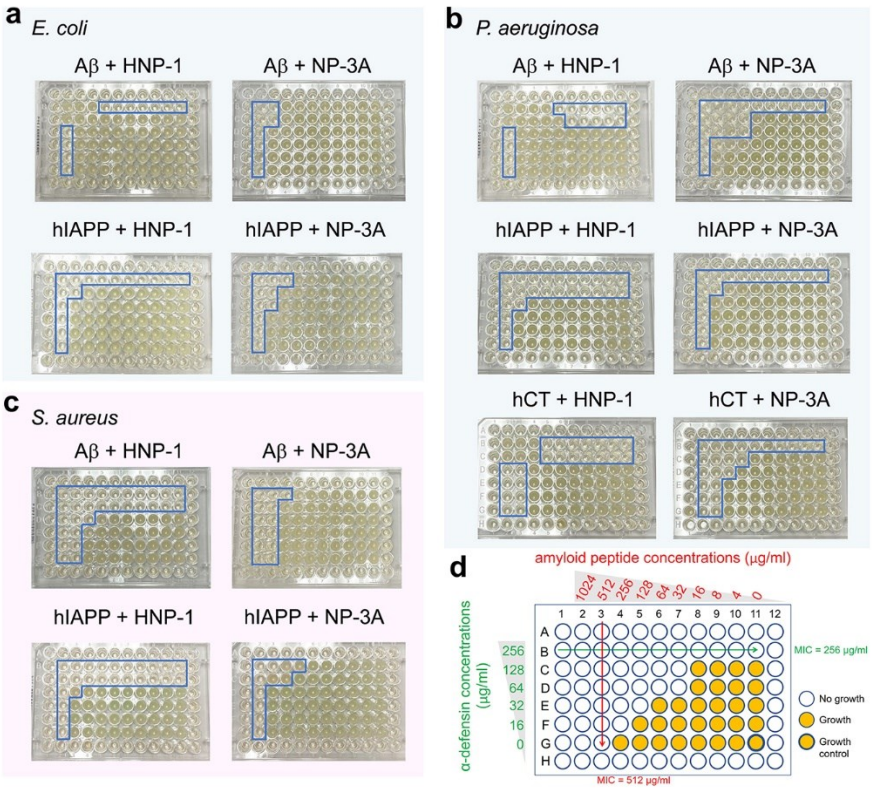

Figure S12. Checkerboard assay for determining the impact on antibacterial potency of the combination of α-defensins and amyloid peptides in comparison to their individual activities.

Antimicrobial activity of α-defensins, amyloid peptides, and combination of α-defensins and amyloid peptides against Gram-negative **a** *E. coli*, **b** *P. aeruginosa*, and **c** Gram-positive *S. aureus* assessed by 2-fold serial dilutions of α-defensins and amyloid peptides in 96-well plate. Wells with bacteria in no growth are determined by OD_{600} of <10% that of a pure bacteria growth control after 20 h growth and are marked in blue boxes. **d** Synergy checkerboard assay setup that includes 2-fold serial dilutions of amyloid peptides from 1024 to 4 μg/ml in each column and α-defensins from 256-16 μg/ml in each row.

Table S1. Inhibition performance of different amyloid inhibitors.

	No.	Inhibitor	Amyloid	Molar Ratio*	Cytotoxicity Reduction	Reference
Sequence-Specific Inhibitors	*1*	Polyphenol phtalocyanine tetrasulfonate (PcTS)	α-synuclein	15	25%	Nat. Comm. 2014 [1]
	2	Cyclic $_{D,L}$-α-peptides	Aβ	10	55%	J. Am. Chem. Soc. 2013[2]
	3	Squalamine	α-synuclein	10	79%	PNAS 2017[3]
	4	Carbazole-based fluorophore SLOH	Aβ	5	30%	Angew. Chem. 2012[4]
	5	Tolcapone Tafamidis	Transthyretin	5 10	50% 40%	Nat. Comm. 2016[5]
	6	Aminopyrazole Trimer Derivatives	Aβ	6	~100%	J. Am. Chem. Soc. 2011[6]
	7	β casein coated AuNPs	Aβ	2.5	69%	Nat. Comm. 2019[7]
	8	Foldamers	Aβ	1	~100%	J. Am. Chem. Soc. 2017[8]
	9	Pt(II)-1,10-phenanthroline complexes	Aβ	1	60-100%	PNAS, 2008[9]
	10	$_{D}$-peptide	Tau	1	*N/A*	Nature 2011[10]
	11	BRICHOS domain of Bri2	hIAPP	1	*N/A*	PNAS 2018[11]
	12	Adapalene	Aβ	1	31%	PNAS 2017[12]
	13	β-wrapin AS69	α-synuclein	1	83%	Angew. Chem. 2014[13]
	14	mimics of the IAPP cross-amyloid interaction surface with Aβ	Aβ	1	88%	Angew. Chem. 2015[14]
	15	Amyloid β-sheet mimics ABSM 1a	Aβ	1	33%	Nat. Chem. 2012[15]
		ABSM 1m	β_2-microglobulin	1	N/A	
		ABSM 1o	α-synuclein	0.5	N/A	
	16	Double N-methylated IAPP analog	hIAPP	1	77%	PNAS 2006[16]
	17	VQIINK inhibitors	Tau	0.4	N/A	Nat. Chem. 2018[17]
	18	Globular protein fused α-syn	α-synuclein	0.1	N/A	Angew. Chem. 2018[18]
	19	Gammabody inhibitor	Aβ	0.1	~100%	PNAS 2012[19]
Dual Inhibitors	*20*	Rhodanine-based molecule 1	hIAPP Tau	>10 >10	N/A 30%	Angew. Chem. 2007 [20]
	21	Rhodanine-based molecule 2	hIAPP Tau	>10 1	N/A 31%	Angew. Chem. 2008[21]

	22	macrocyclic peptides 1a	Aβ	1	80%	Angew. Chem. 2018[22]
		2a		2	60%	
		1a	hIAPP	1	88%	
		2a		2	56%	
	23	Cucurbit[7]uril	Aβ	>10	50%	Angew. Chem. 2014[23]
			insulin	0.5	~100%	
	24	Cathelicidin LL-37	Aβ	1	86%	J Alzheimers Dis. 2017[24]
	25		hIAPP	1	55%	Angew. Chem. 2020[25]
	26	N-methylated IAPP mimics	Aβ	1	42%	Angew. Chem. 2013[26]
			hIAPP	1	55%	
Broad-Spectrum Inhibitors	*27*	Lysine-specific molecular tweezers	Transthyretin	10	~100%	J. Am. Chem. Soc. 2011[27]
			β_2-microglobulin	10		
			Calcitonin	10		
			hIAPP	1		
			Aβ	10		
			Tau	1		

***** Molar ratio: molar ratio of inhibitor to amyloid peptide that completely suppress amyloid aggregation.

Supplementary References

1. Fonseca-Ornelas, L., Eisbach, S. E., Paulat, M., Giller, K., Fernández, C. O., Outeiro, T. F., Becker, S., and Zweckstetter, M. (2014) Small molecule-mediated stabilization of vesicle-associated helical α-synuclein inhibits pathogenic misfolding and aggregation, *Nature communications 5*, 1-11.
2. Richman, M., Wilk, S., Chemerovski, M., Wärmländer, S. K., Wahlström, A., Gräslund, A., and Rahimipour, S. (2013) In vitro and mechanistic studies of an antiamyloidogenic self-assembled cyclic d, l-α-peptide architecture, *Journal of the American Chemical Society 135*, 3474-3484.
3. Perni, M., Galvagnion, C., Maltsev, A., Meisl, G., Müller, M. B., Challa, P. K., Kirkegaard, J. B., Flagmeier, P., Cohen, S. I., and Cascella, R. (2017) A natural product inhibits the initiation of α-synuclein aggregation and suppresses its toxicity, *Proceedings of the National Academy of Sciences 114*, E1009-E1017.
4. Yang, W., Wong, Y., Ng, O. T., Bai, L. P., Kwong, D. W., Ke, Y., Jiang, Z. H., Li, H. W., Yung, K. K., and Wong, M. S. (2012) Inhibition of Beta-Amyloid Peptide Aggregation by Multifunctional Carbazole-Based Fluorophores, *Angewandte Chemie 124*, 1840-1846.
5. Sant'Anna, R., Gallego, P., Robinson, L. Z., Pereira-Henriques, A., Ferreira, N., Pinheiro, F., Esperante, S., Pallares, I., Huertas, O., Rosário Almeida, M., Reixach, N., Insa, R., Velazquez-Campoy, A., Reverter, D., Reig, N., and Ventura, S. (2016) Repositioning tolcapone as a potent inhibitor of transthyretin amyloidogenesis and associated cellular toxicity, *Nature Communications 7*, 10787.
6. Hochdörffer, K., März-Berberich, J., Nagel-Steger, L., Epple, M., Meyer-Zaika, W., Horn, A. H., Sticht, H., Sinha, S., Bitan, G., and Schrader, T. (2011) Rational design of β-sheet ligands against Aβ42-induced toxicity, *Journal of the American Chemical Society 133*, 4348-4358.
7. Javed, I., Peng, G., Xing, Y., Yu, T., Zhao, M., Kakinen, A., Faridi, A., Parish, C. L., Ding, F., Davis, T. P., Ke, P. C., and Lin, S. (2019) Inhibition of amyloid beta toxicity in zebrafish with a chaperone-gold nanoparticle dual strategy, *Nature Communications 10*, 3780.
8. Kumar, S., Henning-Knechtel, A., Chehade, I., Magzoub, M., and Hamilton, A. D. (2017) Foldamer-mediated structural rearrangement attenuates Aβ oligomerization and cytotoxicity, *Journal of the American Chemical Society 139*, 17098-17108.
9. Barnham, K. J., Kenche, V. B., Ciccotosto, G. D., Smith, D. P., Tew, D. J., Liu, X., Perez, K., Cranston, G. A., Johanssen, T. J., Volitakis, I., Bush, A. I., Masters, C. L., White, A. R., Smith, J. P., Cherny, R. A., and Cappai, R. (2008) Platinum-based inhibitors of amyloid-β as therapeutic agents for Alzheimer's disease, *Proceedings of the National Academy of Sciences 105*, 6813-6818.
10. Sievers, S. A., Karanicolas, J., Chang, H. W., Zhao, A., Jiang, L., Zirafi, O., Stevens, J. T., Münch, J., Baker, D., and Eisenberg, D. (2011) Structure-based design of non-natural amino-acid inhibitors of amyloid fibril formation, *Nature 475*, 96-100.
11. Oskarsson, M. E., Hermansson, E., Wang, Y., Welsh, N., Presto, J., Johansson, J., and Westermark, G. T. (2018) BRICHOS domain of Bri2 inhibits islet amyloid polypeptide (IAPP) fibril formation and toxicity in human beta cells, *Proceedings of the National Academy of Sciences 115*, E2752-E2761.
12. Habchi, J., Chia, S., Limbocker, R., Mannini, B., Ahn, M., Perni, M., Hansson, O., Arosio, P., Kumita, J. R., Challa, P. K., Cohen, S. I. A., Linse, S., Dobson, C. M., Knowles, T. P. J., and Vendruscolo, M. (2017) Systematic development of small molecules to inhibit specific microscopic steps of Aβ42 aggregation in Alzheimer's disease, *Proceedings of the National Academy of Sciences 114*, E200-E208.
13. Mirecka, E. A., Shaykhalishahi, H., Gauhar, A., Akgül, Ş., Lecher, J., Willbold, D., Stoldt, M., and Hoyer, W. (2014) Sequestration of a β-Hairpin for Control of α-Synuclein Aggregation, *Angewandte Chemie International Edition 53*, 4227-4230.
14. Andreetto, E., Malideli, E., Yan, L. M., Kracklauer, M., Farbiarz, K., Tatarek-Nossol, M., Rammes, G., Prade, E., Neumüller, T., and Caporale, A. (2015) A Hot-Segment-Based Approach for the Design of Cross-Amyloid Interaction Surface Mimics as Inhibitors of Amyloid Self-Assembly, *Angewandte Chemie International Edition 54*, 13095-13100.
15. Cheng, P.-N., Liu, C., Zhao, M., Eisenberg, D., and Nowick, J. S. (2012) Amyloid β-sheet mimics that antagonize protein aggregation and reduce amyloid toxicity, *Nature chemistry 4*, 927.

16. Yan, L.-M., Tatarek-Nossol, M., Velkova, A., Kazantzis, A., and Kapurniotu, A. (2006) Design of a mimic of nonamyloidogenic and bioactive human islet amyloid polypeptide (IAPP) as nanomolar affinity inhibitor of IAPP cytotoxic fibrillogenesis, *Proceedings of the National Academy of Sciences 103*, 2046-2051.
17. Seidler, P., Boyer, D., Rodriguez, J., Sawaya, M., Cascio, D., Murray, K., Gonen, T., and Eisenberg, D. (2018) Structure-based inhibitors of tau aggregation, *Nature chemistry 10*, 170.
18. Shvadchak, V. V., Afitska, K., and Yushchenko, D. A. (2018) Inhibition of α-Synuclein Amyloid Fibril Elongation by Blocking Fibril Ends, *Angewandte Chemie International Edition 57*, 5690-5694.
19. Ladiwala, A. R. A., Bhattacharya, M., Perchiacca, J. M., Cao, P., Raleigh, D. P., Abedini, A., Schmidt, A. M., Varkey, J., Langen, R., and Tessier, P. M. (2012) Rational design of potent domain antibody inhibitors of amyloid fibril assembly, *Proceedings of the National Academy of Sciences 109*, 19965-19970.
20. Bulic, B., Pickhardt, M., Khlistunova, I., Biernat, J., Mandelkow, E.-M., Mandelkow, E., and Waldmann, H. (2007) Rhodanine-Based Tau Aggregation Inhibitors in Cell Models of Tauopathy, *Angewandte Chemie International Edition 46*, 9215-9219.
21. Mishra, R., Bulic, B., Sellin, D., Jha, S., Waldmann, H., and Winter, R. (2008) Small-Molecule Inhibitors of Islet Amyloid Polypeptide Fibril Formation, *Angewandte Chemie International Edition 47*, 4679-4682.
22. Spanopoulou, A., Heidrich, L., Chen, H. R., Frost, C., Hrle, D., Malideli, E., Hille, K., Grammatikopoulos, A., Bernhagen, J., and Zacharias, M. (2018) Designed macrocyclic peptides as nanomolar amyloid inhibitors based on minimal recognition elements, *Angewandte Chemie 130*, 14711-14716.
23. Lee, H. H., Choi, T. S., Lee, S. J. C., Lee, J. W., Park, J., Ko, Y. H., Kim, W. J., Kim, K., and Kim, H. I. (2014) Supramolecular Inhibition of Amyloid Fibrillation by Cucurbit[7]uril, *Angewandte Chemie International Edition 53*, 7461-7465.
24. De Lorenzi, E., Chiari, M., Colombo, R., Cretich, M., Sola, L., Vanna, R., Gagni, P., Bisceglia, F., Morasso, C., and Lin, J. S. (2017) Evidence that the human innate immune peptide LL-37 may be a binding partner of amyloid-β and inhibitor of fibril assembly, *Journal of Alzheimer's Disease 59*, 1213.
25. Armiento, V., Hille, K., Naltsas, D., Lin, J. S., Barron, A. E., and Kapurniotu, A. (2020) The Human Host-Defense Peptide Cathelicidin LL-37 is a Nanomolar Inhibitor of Amyloid Self-Assembly of Islet Amyloid Polypeptide (IAPP), *Angewandte Chemie International Edition*.
26. Yan, L. M., Velkova, A., Tatarek-Nossol, M., Rammes, G., Sibaev, A., Andreetto, E., Kracklauer, M., Bakou, M., Malideli, E., and Göke, B. (2013) Selectively N-Methylated Soluble IAPP Mimics as Potent IAPP Receptor Agonists and Nanomolar Inhibitors of Cytotoxic Self-Assembly of Both IAPP and Aβ40, *Angewandte Chemie International Edition 52*, 10378-10383.
27. Sinha, S., Lopes, D. H. J., Du, Z., Pang, E. S., Shanmugam, A., Lomakin, A., Talbiersky, P., Tennstaedt, A., McDaniel, K., Bakshi, R., Kuo, P.-Y., Ehrmann, M., Benedek, G. B., Loo, J. A., Klärner, F.-G., Schrader, T., Wang, C., and Bitan, G. (2011) Lysine-Specific Molecular Tweezers Are Broad-Spectrum Inhibitors of Assembly and Toxicity of Amyloid Proteins, *Journal of the American Chemical Society 133*, 16958-16969.